ACS OMEGA

http://pubs.acs.org/journal/acsodf

Article

Substitution of the Methionine Axial Ligand of the T1 Copper for the Fungal-like Phenylalanine Ligand (M298F) Causes Local Structural Perturbations that Lead to Thermal Instability and Reduced Catalytic Efficiency of the Small Laccase from *Streptomyces coelicolor* A3(2)

Kairit Zovo, Hegne Pupart, Arie Van Wieren, Richard E. Gillilan, Qingqiu Huang, Sudipta Majumdar, and Tiit Lukk*

Cite This: *ACS Omega* 2022, 7, 6184–6194

Read Online

ACCESS | Metrics & More | Article Recommendations | Supporting Information

ABSTRACT: Many industrial processes operate at elevated temperatures or within broad pH and salinity ranges. However, the utilization of enzymes to carry out biocatalysis in such processes is often impractical or even impossible. Laccases (EC 1.10.3.2), which constitute a large family of multicopper oxidases, have long been used in the industrial setting. Although fungal laccases are in many respects considered superior to their bacterial counterparts, the bacterial laccases have been receiving greater attention recently. Albeit lower in redox potential than fungal laccases, bacterial laccases are commonly thermally more stable, act within broader pH ranges, do not contain posttranslational modifications, and could therefore serve as a high potential scaffold for directed evolution for the production of enzymes with enhanced properties. Several examples focusing on the axial ligand mutations of the T1 copper site have been published in the past. However, structural evidence on the local and global changes induced by those mutations have thus far been of computational nature only. In this study, we set out to structurally and kinetically characterize a few of the most commonly reported axial ligand mutations of a bacterial small laccase (SLAC) from *Streptomyces coelicolor*. While one of the mutations (Met to Leu) equips the enzyme with better thermal stability, the other (Met to Phe) induces an opposite effect. These mutations cause local structural rearrangement of the T1 site as demonstrated by X-ray crystallography. Our analysis confirms past findings that for SLACs, single point mutations that change the identity of the axial ligand of the T1 copper are not enough to provide a substantial increase in the catalytic efficiency but can in some cases have a detrimental effect on the enzyme's thermal stability parameters instead.

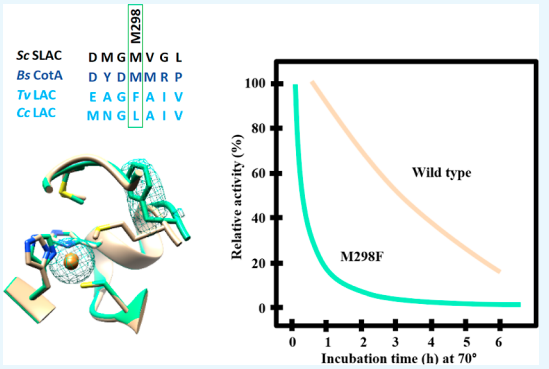

INTRODUCTION

Laccases (EC 1.10.3.2) are multicopper oxidases that catalyze the oxidation of various aromatic compounds by the concomitant four-electron reduction of molecular oxygen to water.[1−3] Laccases are widespread in nature with diverse functions. They are found in plants, fungi, some insects, and bacteria. In plants, laccases participate in lignin synthesis, wound healing, and iron oxidation. In fungi, laccases have roles in lignin degradation, morphogenesis, pigmentation, and pathogenesis. In insects, their function is in sclerotization of cuticles and in bacteria, they participate in morphogenesis, pathogenicity, melanin formation, and copper homeostasis.[1,4,5]

For enzymatic activity, laccases require four copper atoms, distributed between copper centers—a mononuclear and a trinuclear copper cluster. Copper coordinating ligands are conserved among the species.[4,6,7] Active site coppers are divided into three types according to their spectroscopic and paramagnetic properties. The Type-1 (T1) copper has a trigonal coordination with two histidine residues and one cysteine residue. In addition, it has a weakly coordinating or non-coordinating residue in the axial position. Laccases that have a non-coordinating residue (Phe or Leu) in the axial position (fungal laccases) generally have higher redox potential values compared to their bacterial counterparts.[8] Type 2 (T2) and two Type 3 (T3) copper ions form a trinuclear cluster

Received: November 24, 2021
Accepted: January 28, 2022
Published: February 9, 2022

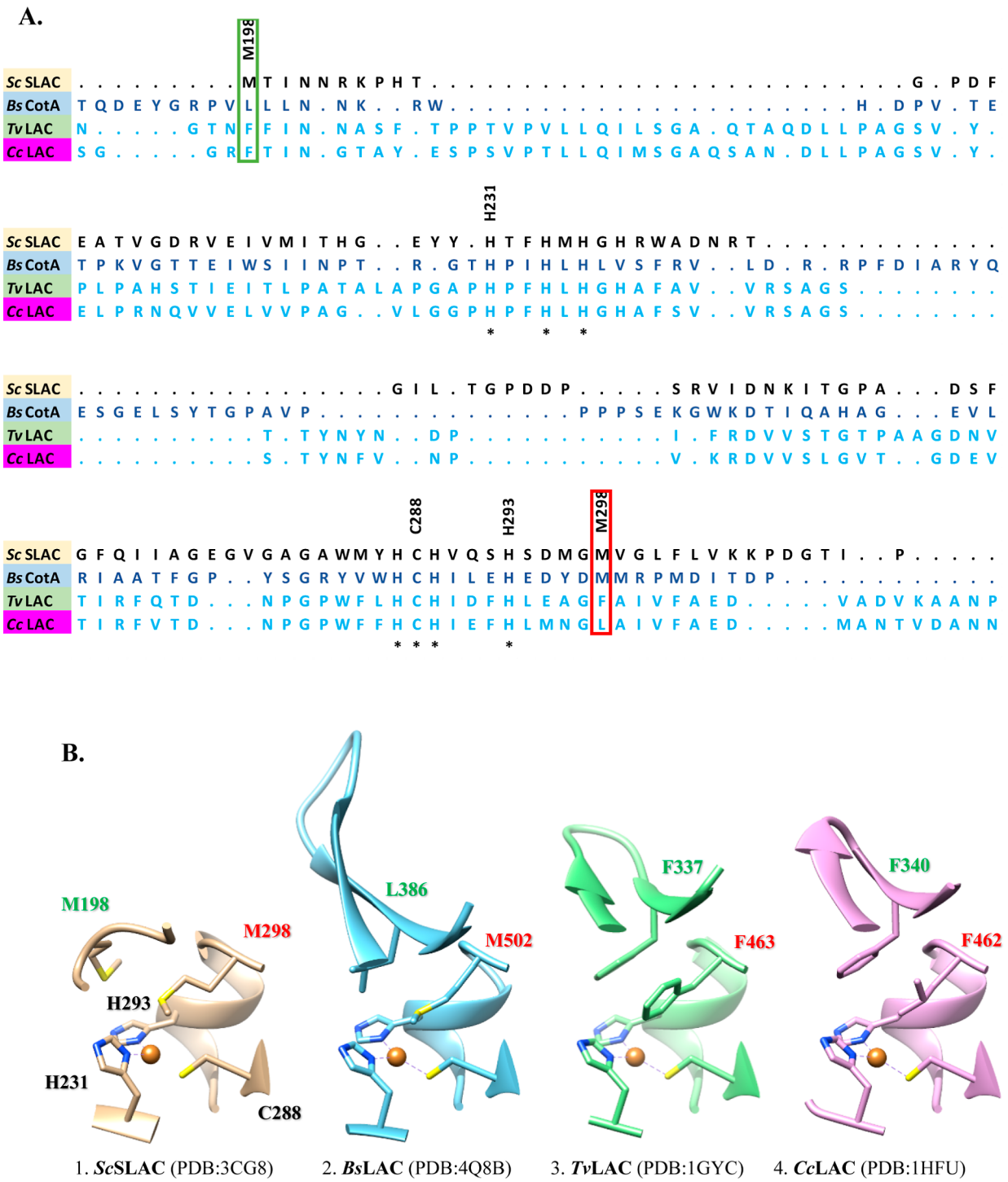

Figure 1. (A) Partial structure-based multiple sequence alignment of the mononuclear copper site of two bacterial (2-domain *S. coelicolor* and 3-domain *B. subtilis*) and two fungal laccases (2-domain from *T. versicolor* and *C. cinereus*). The axial ligand to the T1 copper is highlighted with a red box and its stabilizing interaction partner with a green box; (B) T1 copper interaction partners for the small and large laccases from bacteria and fungi; axial ligand and their stabilizing interaction partner are in red and green, respectively.

(TNC) and are coordinated by eight histidine residues. The substrate is oxidized near the T1 site, electrons are then transferred one by one along a pathway containing Cys and His residues to the TNC, where molecular oxygen is reduced to water.[1,2]

The most studied laccases are of fungal origin, having three domains and are monomeric. In 2004, Machczynski et al. described a structurally different laccase from soil bacteria *Streptomyces coelicolor* containing two domains per monomer. The new type of laccase was named the small laccase (SLAC). The SLAC from the soil dwelling actinomycete *S. coelicolor* (*Sc*SLAC) also utilizes four copper atoms distributed between the two clusters and the copper coordinating ligands are located in the same relative positions as compared to other laccases.[9] The active form of *Sc*SLAC is homotrimeric, containing 12 copper atoms per trimer. The T1 copper atom

https://doi.org/10.1021/acsomega.1c06668
ACS Omega 2022, 7, 6184−6194

is located in domain 2 and the TNC is located at the interface of domain 1 and 2 of the neighboring polypeptide chains, structurally mimicking the domains 2 and 3 of the large laccase from fungi.[10]

Both fungal and bacterial laccases have broad substrate specificities making them suitable for various biotechnological and industrial applications.[5,11,12] Therefore, laccases have been extensively studied as the eco-friendly (water as the only byproduct) multipurpose enzymes to replace conventional industrial methods with sustainable approaches to reduce the environmental impact. Fungal laccases are industrially used for diverse purposes. In food industry, they are used as stabilizers or additives to improve food sensory parameters and in textile industry as a bleaching agent or to dye fabrics with heteropolymeric dyes.[12] Fungal laccases are not only used in organic synthesis to synthesize pharmacologically important compounds but also find uses in bioremediation, cosmetics, nanotechnology, and biomedicine.[5,12,13] Additionally, laccases have been studied for their potential in biomass pretreatment for enzymatic delignification in biorefinery or as a substitute for some of the chemical catalysts required for pulp and paper processing.[8,14]

Fungal laccases, in general, have higher redox potentials than bacterial laccases,[15,16] yet bacterial laccases have wide pH tolerance range, better tolerance of elevated temperatures, increased tolerance to different organic solvents and metal ions, which makes them attractive candidates for industrial uses.[11,13,17−19] Increasing number of studies are showing that bacterial laccases can be useful for industrial applications. Bacterial laccases have been studied to carry out decolorization of dyes (textile industry) and pollutant degradation (bioremediation).[13] Bacterial laccases can be useful in paper pulp bio-bleaching and wastewater treatment[19] as well as biomass delignification.[11,20] In addition to treating grassy biomass, laccases from *Streptomyces* could potentially to be useful in lignin degradation from woody biomass as well. *Sc*SLAC was implicated in the ability to depolymerize lignin from *Miscanthus x giganteus* by increasing the amount of acid-precipitable polymeric lignin (APPL) in its growth environment.[21] SLAC from *Amycolatopsis* sp. 75iv3 was able to degrade steam-pretreated poplar by increasing the amount of APPL while leading to the reduction of its molecular weight by 50%.[22] Bacterial strains harboring the genes that encode laccases have been studied as promising tools for large-scale utilization and conversion of lignin to more valuable products.[19,23] However, the oxidizing potential of bacterial laccases on lignin depolymerization is not high enough to meet the industrial needs. Further optimization using molecular biology tools is therefore necessary. Several studies have shown that the redox potential of laccases can be tuned and the range of catalytically active substrates increased by rational design.[15,24−30] Using molecular dynamics simulations, Hong et al. predicted that the replacement of the axial Met residue in *Sc*SLAC would increase the redox potential of that enzyme.[25] One of the main targets has been the T1 Cu site and modifications in its immediate vicinity for catalytic improvement.[8] The idea of tuning the redox potential of enzymes belonging to the cupredoxin fold by modifying the identity of just the axial ligand of the T1 copper is not new and substitution of that residue has been proven as an effective measure for the enzymes' overall catalytic improvement.[31,32]

Additionally, Sherif et al. used site-directed mutagenesis to mutate 17 amino acid residues, including 10 histidine residues, a cysteine, and a methionine residue from the copper coordination sphere of *Sc*SLAC. All the mutations reduced enzyme activity, confirming the importance of copper coordinating residues. M298A mutation reduced the enzyme activity by 35%. The Y229A and Y230A mutants showed over 10-fold increase in activity compared with the wild type laccase.[18] Gupta et al. investigated the role of Y108 in *Sc*SLAC. Y108A and Y108F mutations reduced the turnover number but did not affect the catalytic efficiency. Y108 is situated ∼5 Å away from the T2 Cu ion and is involved in oxygen reduction.[33] Prins et al. mutated the axial M298 T1 copper ligand of *Sc*SLAC to phenylalanine, which decreased the turnover rate and overall efficiency; however, the enzyme showed higher efficiency at temperatures above 70 °C.[17]

The aim of the current study was to gain structural insights into the previously characterized mutants of the axial ligand to the T1 copper. In addition to re-investigating their kinetic parameters at elevated temperatures, we report lowered resistance to elevated temperatures in longer time-course experiments than what had been reported in previous studies. Here, we determined the X-ray crystal structures of M298F and M298L single mutants (to 2.2 Å resolution), and the M198F M298F double mutant (to 2.0 Å resolution) to study the effects of mutagenesis induced local displacements around the T1 copper site. We also performed small angle X-ray scattering (SAXS) to identify possible larger scale motions that would have possibly been frozen out due to crystal packing interactions.

RESULTS

Determination of Local Structural Displacements. The first crystal structure of the bacterial SLAC was published in 2009.[10] Since then, several attempts have been made to increase the catalytic efficiency and thermal stability of the SLACs via structure guided site-directed mutagenesis. Multiple sequence alignments of the high redox potential large laccases from fungi and of bacterial laccases reveal that copper binding residues at the T1 and T2/T3 sites are highly conserved. However, one distinct feature that differentiates the low redox potential enzymes from the more efficient fungal counterparts—the identity of the axial ligand to the T1 copper (Figure 1A,B). Several examples can be found from the literature that deal explicitly with mutations to the T1 copper site for enhanced function.[25,27,30] It has been hypothesized that the identity of the axial ligand may be one of the key determinants in tuning the redox potential of the enzyme.[34] However, thus far only one crystal structure of an axial ligand mutant[35] of a SLAC and a few computational models[25] have been published. Motivated by the scarcity of structural information, we set out to determine if and how the changes in the axial ligand identity of the SLAC affect the enzyme structurally in local and global context that may serve to explain the rather modest gains or even losses in activity/redox potential and the loss of thermal stability of those mutants.

Here, we solved the X-ray crystal structures of the T1 copper axial ligand mutants of *Sc*SLAC, where the identity of the mutated residues was chosen based on previously determined crystal structures of high redox potential fungal laccases: leucine for *Coprinus cinereus* (*Cc*LAC)[36] and phenylalanine for *Trametes versicolor* (*Tv*LAC).[37] As all structures of the mutant enzymes under study were solved in the cubic $P2_13$ lattice, for comparison accuracy, the structure of the wild-type *Sc*SLAC was re-determined in the same point group symmetry as to

https://doi.org/10.1021/acsomega.1c06668
ACS Omega 2022, 7, 6184−6194

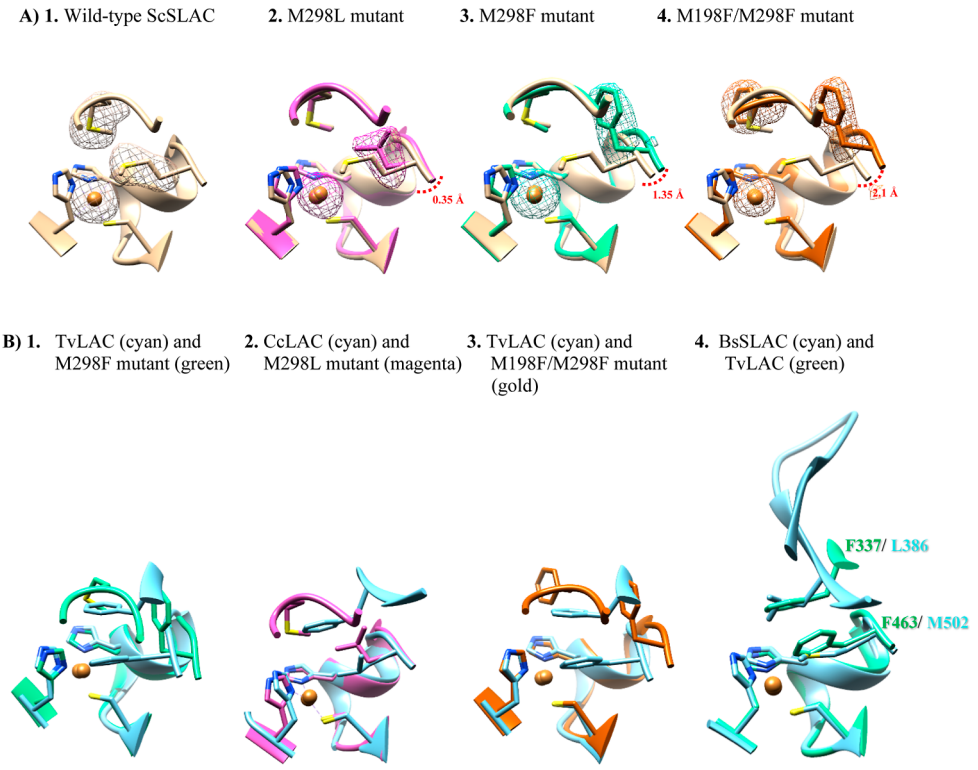

Figure 2. (A) From left to right: omit maps from the T1 copper site (contoured at 4σ above background) calculated with the Fourier coefficients ($F_{obs} - F_{calc}$) with phases from the final models but with the coordinates of the M198/M298/Cu (wild type, beige), L298/Cu (M289L mutant, magenta), F298/Cu (M298F mutant, green), and F198/M298/Cu (M198F/M298F double mutant, gold) omitted prior to calculations, respectively. The coordinates of the final models of mutants are superimposed with corresponding maps and with the coordinates of wild-type ScSLAC for comparison accuracy. Displacement distance between the C_α-s of the mutated axial ligand are marked with a contoured line. (B) Overlays of the poses for the T1 site of (1) *Tv*LAC with M298F mutant (cyan-green), (2) *Cc*LAC with M298L mutant (cyan-magenta), (3) *Tv*LAC with M198F/M298F double mutant (cyan/gold), and (4) *Bs*LAC with TvLAC (cyan-green).

exclude the possibility of differences arising from alternative crystal packing of the previously published structures.[10,38] Substitution of the methionine axial ligand of the wild type *Sc*SLAC for a branched hydrophobic leucine or an aromatic phenylalanine moiety introduced a loop displacement where instead of the expected cation−hydrophobic interaction or a cation−π interaction, we see the ligand shift away from the catalytic metal ion.

More specifically, in case of the M298F mutation, where the structural effects are more pronounced, the loop carrying the axial ligand is displaced by 1.35 Å when measuring distances of the C_α-s of residue 298 between wild type and mutant enzyme (Figure 2A4). When comparing the distances of C2 of the phenylalanine ring of F463 of *Tv*LAC to the T1 copper with the respective C2 of the M298F mutant, the distance increases from 3.65 Å (*Tv*LAC) to 6.72 Å (M298F) swinging the phenylalanine side chain completely out of the view and leaving the T1 site relatively open to solvent (Figure 2B1). The M298L mutation, which mimics the T1 site of *Cc*LAC has a less pronounced effect on the movement of the same loop—0.35 Å between C_α-s of WT and M298L mutant (Figure 2). The distance of the C_α of the leucine residue to T1 copper is elongated to 4.36 Å when compared to the L462-C_α to T1 copper distance of 3.5 Å of in *Cc*LAC (Figure 2B2). Prior to having solved the crystal structure of the M298F mutant, we hypothesized that M198 could serve as the spatial homolog of F337 of *Tv*LAC. In the *Tv*LAC structure (PDB code 1GYC), the axial ligand of T1 copper F463 is stabilized via a weak $\pi-\pi$ stacking interaction with F337 (Figure 1B3). We therefore hypothesized that a double mutant of M198F M298F might be able to mimic that interaction and similarly lead to stabilization of the axial ligand. The structural homolog of that phenylalanine (F340) is conserved in *Cc*LAC and forms a hydrophobic interaction with the axial L462 (Figure 1B4). In spite of our expectations to see those phenylalanines complementing each other, there is an even greater displacement of the loop carrying the axial ligand in the M198F M298F mutant by almost 2.1 Å between C_α-s of position 298 (Figure 2A4). Albeit M198F remained in place and C2 of the phenylalanine ring aligns with the sulfur of the methionine side chain, M298F is swung back even further, where the C2 of the M298F phenyl ring distance from T1 copper measures 7.66 Å (Figure 2B3). Therefore, rather unexpectedly, the introduction of a bulky hydrophobic residue into *Sc*SLAC in place of the methionine axial ligand introduces an unwanted displacement of its carrying loop and destabilizes that local region.

In contrast to substitutions such as these having been demonstrated as a viable strategy to improve a bacterial large laccase,[24] *Sc*SLAC likely requires additional tweaking of the surroundings of the axial ligand to accept a bulky hydrophobic residue in that position. Likely, the reason why the axial ligand substitution worked for the three-domain laccase from *Bacillus subtilis* is because it contains the structural homolog of F337 of *Tv*LAC or F340 of *Cc*LAC, which in case of the CotA laccase is a leucine and occupies the same structural space as the fungal enzymes (Figure 2B4). The replacement of the axial methionine residue with a hydrophobic leucine that is similar in size to the original methionine moiety does not disturb, nor

https://doi.org/10.1021/acsomega.1c06668
ACS Omega 2022, 7, 6184−6194

introduce novel interactions that would otherwise lead to major displacements in its local environment. It has been reported that the methionine to leucine mutation in bacterial SLACs results only in modest gains in the redox potential of the T1 center.[24,35] Although hydrophobic interactions or the introduction of those therein can be useful in tuning the redox potentials of T1 copper centers,[39] our analysis confirms past findings[24,35] that a single point mutation alone in the primary coordination sphere of the T1 copper center is not enough to achieve substantially increased redox potential or enhanced catalytic activity of *Sc*SLAC. Such mutations can instead have detrimental effects on the catalytic efficiency of the enzyme and on its overall thermal stability.[18] The unsuitability of the local environment to accept a bulky hydrophobic residue in the axial position becomes clear from the solved X-ray crystal structures as undesirable changes in the local environment become visible when comparing mutants to the wild-type enzymes of the mutation templates (i.e., fungal enzymes) (Figure 2B1−3).

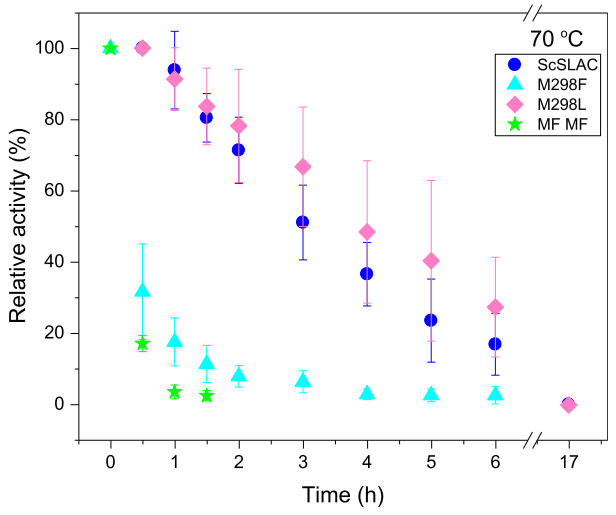

Figure 3. Heat inactivation profiles as determined for wild type and axial ligands in the presence of ABTS substrate at 70 °C. Some level of protection against heat-inactivation can be achieved by mutating the axial Met (blue circles) to a Leu residue (pink circles). Double mutant of M198F/M298F (MFMF) is the most susceptible to heat inactivation.

Probing for Global Perturbations. X-ray crystal structures are typically considered as rigid snapshots of protein molecules that have been constrained into a crystal lattice, which remains particularly constrained when considering cryo-crystallography. Carrying out crystallographic experiments at elevated temperatures will unfreeze some conformational states (rotameric, local loop movements) within the protein crystal structure which do not translate to observable large-scale domain motions due to crystal packing.[40] In order to produce a version of the SLAC in its most native form possible, we tested two alternative methods for bacterial cell lysis. Although many consider the French press as the mild go-to method for cell lysis as the sample experiences little to no thermal changes during the cell lysis, pressure differences required for the complete and effective disruption of bacterial cells are in the order of 1 kbar. Albeit not widely reported, some proteins can undergo pressure induced denaturation.[41] Thus, for SAXS experiments, we set out to test two sets of protein samples—those from lysis performed at an ambient pressure over ice using sonication and those from using the French press for lysis at ambient temperature. In this study, we refer to wild-type sonicated sample as "WTS" and wild-type French press sample as "WTF." Similarly, mutants that are either sonicated or subjected to the French press have an "S" or "F" appended, respectively. Thus, M298F is referred to as "MFS" or "MFF" and M298L is referred to as "MLS" or "MLF."

Size-exclusion chromatography-coupled SAXS was performed on all samples to confirm sample purity and produce buffer-subtracted profiles free from radiation damage. Single symmetric elution peaks were observed with radii of gyration that were visually indistinguishable among the five samples and level throughout the peaks (Figure S1). The samples varied somewhat in concentration (elusion peak height) with the wild type being the most dilute. The Guinier plots of the profiles are linear and show no obvious systematic deviations that would indicate aggregation or concentration effects (Figure S2).

To make a more precise statistical comparison, all profiles were aligned by scaling to equivalent $I(0)$ values and the χ^2 statistic was subsequently calculated relative to the wild type (WTS). As a result, χ^2 = 1.06 (WTS-WTF), 1.18 (MFF-WTF), 1.31 (MFS-WTF), 1.13 (MLF-WTF), and 1.37 (MLS-WTF). Though close to unity, the χ^2 values suggest that sonication may introduce some changes in the mutant profiles. Radii of gyration computed by the Guinier analysis were R_g = 30.10 ± 0.07 Å (WTF), 30.03 ± 0.11 Å (WTS), 30.13 ± 0.06 Å (MFF), 30.15 ± 0.04 Å (MFS), 30.18 ± 0.05 Å (MLF), and 30.28 ± 0.04 Å (MLS). The error bounds here are based on the Guinier linear fit and represent approximately ± 1 standard deviation. In Figure 4, the wild-type and M298F mutants show

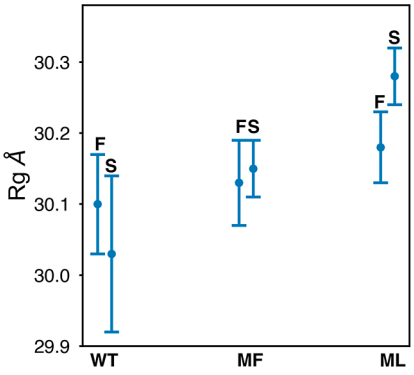

Figure 4. Radii of gyration (R_g) with ± 1 σ for error bars for wild-type (WT) and mutants (M298F, M298L) with a side-by-side comparison of sonication (S) and the French press (F) treatments. The M298L mutant, which appears to have a slightly higher R_g than the other samples, responded differently to the two treatments.

no significant difference in R_g between the sonication and French press treatments. The sonicated M298L mutant (MLS) produces a significantly higher R_g compared to the other samples.

The Kratky plots of the profiles all overlap visually to within the noise limits, are unimodal, and fall back to the baseline at high q-value. This behavior is characteristic of a compact, well-folded globular protein. While the WTF and MLS pairs differ most in both χ^2 and R_g values, their Kratky plots are difficult to distinguish at the current experimental noise level (Figure 5).

Point Mutations Affect Thermal Stability. Because laccases have tremendous potential for industrial use,

https://doi.org/10.1021/acsomega.1c06668
ACS Omega 2022, 7, 6184−6194

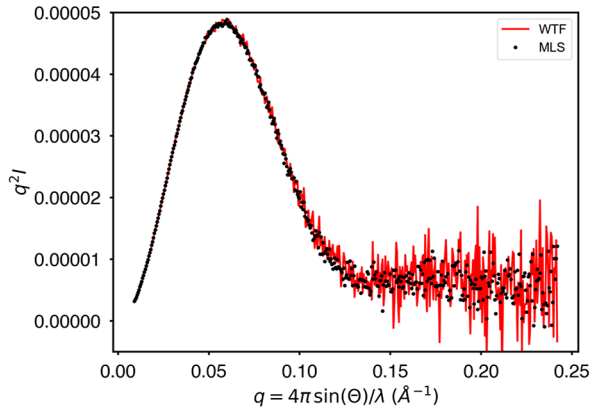

Figure 5. Kratky plot of the wild type French pressed protein (WTF) compared to the M298L mutant prepared by sonication (MLS). Though the two curves differ slightly according to the radius and gyration and χ^2 (1.36), the profiles are difficult to distinguish at the current level of experimental noise.

improving their catalytic properties for use in environments that operate at elevated temperatures is desirable for biotechnological enzymes to have long-term thermal stability. Structural basis for T1 site instability of the bacterial SLAC in the mutant enzymes seems to stem from the generally less hydrophobic local environment of the axial ligand when compared to the large laccases. Comparatively less hydrophobic immediate vicinity of the T1 site in SLACs is likely the reason why substitution of the axial ligand with an increasingly more hydrophobic residue leads to substantial local structural reorganization. Incubation of mutant enzymes at different temperatures for extended periods of time, followed by measurement of relative baseline activity with two model substrates (ABTS and DMP) revealed that only the M298L mutation had protective effects against heat inactivation (Figure 3). Comparing the heat inactivation half-lives ($\tau^{1/2}$) at 70 °C, the relative activity of M298L when compared to wild-type *Sc*SLAC is extended from 3.5 to 5.4 h (Table 1). A

Table 1. Heat-Inactivation Half-Lives ($\tau^{1/2}$) in Hours as Calculated for Wild-Type and Axial Ligand Mutants of the *Sc*SLAC Enzyme[a]

	80 °C	70 °C	60 °C
ScSLAC	1.5 ± 0.2	3.5 ± 0.3	
M298F		0.6 ± 0.1	4.7 ± 0.6
M298L	2.7 ± 0.4	5.4 ± 0.4	
M198F/M298F		0.3 ± 0.01	2.1 ± 0.2

[a]The curves were fitted and standard deviations calculated by the exponential decay function in the OriginPro software package.

two-factor ANOVA test was carried out in order to compare thermal stabilities of the WT enzyme and M298L mutant. ANOVA results confirmed that the difference in activities of the enzymes is statistically significant $F_{crit} < F$ (5.6 < 9.6) at a 0.95 significance level, $p = 0.02$. As for the M298F single and the M198F/M298F double mutant, introduction of the bulky hydrophobic residue decreases the $\tau^{1/2}$ at 70 °C to about a half and a quarter hour, respectively, when compared to the 3.5 h of wild-type. The protective effect of M298L mutation is also measurable at 80 °C, where heat inactivation $\tau^{1/2}$ is extended from 1.5 to 2.7 h when compared with the wild-type enzyme (Figure S3).

Point Mutations to the Axial Ligand Have but Limited Effect on Kinetic Parameters. All of the steady-state kinetics were determined at 42 °C, and even though differences between mutant and wild type enzymes within the limited range of tested substrates exist, these differences can only be considered as mild-to-moderate (Table 2). Previous studies on the axial ligand mutations of *Sc*SLAC, which focused efforts on the determination of redox potentials of those mutants, seem to confirm the notion that only minor effects can be observed in either slightly improved or slightly worsened values. Based on the now available structural info, we hypothesize that these effects can be attributed to the small local structural perturbations that are brought about by hydrophobic−hydrophilic repulsions about the axial ligand and the lack of favorable hydrogen-bonding interaction partners on the peptide backbone of the ligand-carrying loop.

DISCUSSION

Laccases are an important class of enzymes with tremendous potential for use in different industrial processes. While fungal laccases have excellent performance characteristics within a limited pH and temperature range, the bacterial laccases tend to operate in much broader environmental conditions, albeit with poorer performance. Past research studies into the engineering of the SLAC have relied mostly on computational methods and direct measurements of redox potentials as well as enzyme kinetics on common laccase substrates. Here, we have provided first structural insights into the structural perturbations that are brought about due to mutations of the axial ligand. SAXS measurements indicate that the mutations do not alter the global folding or solution state of the protein. The comparison of wild type proteins processed by sonication and the French press do not show any large-scale structural differences in solution. Some subtle structural change is evident the χ^2 statistics for the sonicated M298F and M298L mutants and the difference is further evidenced in the R_g for M298L. However, given the subtle nature of the changes, it is not possible under the current experimental conditions to draw conclusions about the nature of structural changes. The result is consistent with the long-standing view that the French press is gentler on samples than sonication. It may be that mutant proteins less stable than the wild type are more susceptible to harsh treatment. A further study is warranted.

The results from X-ray crystallography combined with thermal stability assays seem to indicate that the larger and more hydrophobic residues not only perturb the local environment of the T1 site but also indicate that there is a fine balance between the distancing of the axial ligand to copper atom and the mutant's thermal stability. The distance of the M298L residue to copper atom is only slightly increased from the position of wild-type's M298—nevertheless a change of this magnitude seems to play a role in improving the enzymes' thermal inactivation half-life. However, a greater distance from the T1 copper atom that can be seen for M298F seems to perturb the local environment so much so that the tight coordination of copper atom is affected at elevated temperatures, resulting in thermal inactivation half-lives seven-fold shorter than with the wild-type enzyme. That effect is even more pronounced for the M198F/M298F double mutant, where the heat-inactivation half-life is reduced by almost thirteen-fold when compared to wild-type enzyme. Having concrete structural information from X-ray crystallography on the active site geometry will therefore enable the establishment

https://doi.org/10.1021/acsomega.1c06668
ACS Omega 2022, 7, 6184−6194

Table 2. Steady State Kinetic Parameters as Determined for Wild Type and Axial Ligand Mutants of the ScSLAC Enzyme at 42 °C[a]

42 °C	ABTS	DMP	Pyrogallol	hydrocoerulignone
ScSLAC	k_{cat} = 38.6 s^{-1}	k_{cat} = 4.2 s^{-1}	k_{cat} = 17.2 s^{-1}	k_{cat} = 11.3 s^{-1}
	K_m = 7.3 ± 0.26 mM	K_m = 1.1 ± 0.06 mM	K_m = 0.2 ± 0.06 mM	K_m = 0.3 ± 0.05 mM
	k_{cat}/K_m = 5.3 × 10^3 s^{-1} M^{-1}	k_{cat}/K_m = 3.8 × 10^3 s^{-1} M^{-1}	k_{cat}/K_m = 8.6 × 10^4 s^{-1} M^{-1}	k_{cat}/K_m = 3.8 × 10^4 s^{-1} M^{-1}
ScSLAC	k_{cat} = 3.7 s^{-1}	k_{cat} = 0.7 s^{-1}	k_{cat} = 21.9 s^{-1}	k_{cat} = 5.4 s^{-1}
M298F	K_m = 4.1 ± 0.24 mM	K_m = 1.2 ± 0.19 mM	K_m = 0.3 ± 0.09 mM	K_m = 0.3 ± 0.05 mM
	k_{cat}/K_m = 0.9 × 10^3 s^{-1} M^{-1}	k_{cat}/K_m = 0.6 × 10^3 s^{-1} M^{-1}	k_{cat}/K_m = 7.3 × 10^4 s^{-1} M^{-1}	k_{cat}/K_m = 1.8 × 10^4 s^{-1} M^{-1}
ScSLAC	k_{cat} = 9.3 s^{-1}	k_{cat} = 1.5 s^{-1}	k_{cat} = 21.9 s^{-1}	k_{cat} = 7.2 s^{-1}
M298L	K_m = 5.0 ± 0.22 mM	K_m = 1.3 ± 0.09 mM	K_m = 0.3 ± 0.12 mM	K_m = 0.3 ± 0.05 mM
	k_{cat}/K_m = 1.9 × 10^3 s^{-1} M^{-1}	k_{cat}/K_m = 1.2 × 10^3 s^{-1} M^{-1}	k_{cat}/K_m = 7.3 × 10^4 s^{-1} M^{-1}	k_{cat}/K_m = 2.4 × 10^4 s^{-1} M^{-1}
ScSLAC	k_{cat} = 3.9 s^{-1}	k_{cat} = 0.8 s^{-1}	k_{cat} = 26.3 s^{-1}	k_{cat} = 5.6 s^{-1}
M198F	K_m = 1.1 ± 0.04 mM	K_m = 1.1 ± 0.08 mM	K_m = 0.5 ± 0.07 mM	K_m = 0.1 ± 0.02 mM
M298F	k_{cat}/K_m = 3.5 × 10^3 s^{-1} M^{-1}	k_{cat}/K_m = 0.7 × 10^3 s^{-1} M^{-1}	k_{cat}/K_m = 5.3 × 10^4 s^{-1} M^{-1}	k_{cat}/K_m = 5.6 × 10^4 s^{-1} M^{-1}

[a]All measurements were carried out in triplicate.

Table 3. Primer Sequences for the Generation of Axial Ligand Mutants of *Sc*SLAC

primer	sequence
ScSLAC-M298F-FP	5′-CGACATGGGCTTCGTGGGGCTGTTC-3′
ScSLAC-M298F-RP	5′-GAGTGGCTCTGGACGTGG-3′
ScSLAC-M298L-FP	5′-CGACATGGGCCTGGTGGGGCTGT-3′
ScSLAC-M298L-RP	5′-GAGTGGCTCTGGACGTGGC-3′
ScSLAC-M198F-FP	5′-CTTCAACGACTTCACCATCAACAACCGCAAG-3′
ScSLAC-M198F-RP	5′-ACGATCGTGTGCGTGGCG-3′

of better parameters on the redesign of SLACs with enhanced thermal and catalytic properties.

MATERIALS AND METHODS

Chemicals. 2,2′-Azino-bis-(3-ethylbenzothiazoline-6-sulphonic acid) diammonium salt (ABTS) was purchased from Alfa Aesar (MA, USA); 2,6-dimethoxyphenol (DMP) from Acros Organics (NJ, USA), pyrogallol, and dimethylformamide were purchased from Fisher Chemical (Loughborough, UK); hydrocoerulignone (HCL) and isopropyl-*β*-D-thiogalactopyranoside (IPTG) were obtained from MP Biomedicals, LCC (Illkirch, France); and dimethyl sulfoxide (DMSO) was purchased from Amresco (Ohio, USA).

Cloning and Mutagenesis of *Sc*SLAC. The gene encoding the SLAC from *S. coelicolor* A3(2) was cloned into pET15b (Novagen) to create the expression vector p15-ScSLAC as described before.[21]

Mutagenesis. The plasmid p15-ScSLAC was used as the DNA template to generate two ScSLAC single mutants M298F and M298L using a Q5 site-directed mutagenesis kit (NEB). The plasmids in Table 1 were used to mutate methionine codon ATG at position 298 to phenylalanine codon TTC and leucine codon CTG, respectively. The PCR mixture (10 μL) contained 1 μL of 10 ng/μL template DNA plasmid, 1 μL each of 5 μM forward and reverse primers, 5 μL of Q5 HS master mix, and 2 μL of ddH_2O. The PCRs were performed in a BioRad T100 thermal cycler with the following parameters: 98 °C for 30 s followed by 25 cycles of 98 °C for 10 s, 70 °C for 20 s and 72 °C for 3 m, and a final extension time of 2 m at 72 °C. The PCR reactions were confirmed by DNA gel electrophoresis. The KLD reactions were performed at room temperature for 10 min with 0.5 μL of the amplified PCR product, 2.5 μL of KLD reaction buffer, 1.5 μL of ddH_2O, and 0.5 μL of KLD enzyme mixture. 2.5 μL of KLD mixtures were chemically transformed into 5-alpha competent *Escherichia coli* cells. The mutations were confirmed by DNA sequencing (Genewiz, USA).

The M198F M298F double mutant was generated following the same protocol as described for single mutant generation using the p15-ScSLAC-M298F single mutant as the PCR template and ScSLAC-M198F-FP and ScSLAC-M198F-RP primers (Table 3).

Protein Expression and Purification. Wild-type *Sc*SLAC and its mutants were expressed in *E. coli* BL21 (DE3) cells (Novagen). Three mL of the starter cultures was inoculated into 500 mL of Luria−Bertani (LB) media containing 100 μg/mL ampicillin. The cultures were incubated at 37 °C with shaking (180 rpm) until OD_{600} = 0.6. Protein expression was induced with IPTG (final concentration 0.5 mM). After induction, the cells were incubated overnight at 30 °C with shaking (180 rpm). Cells were harvested by centrifugation (Beckman Coulter Avanti; rotor: JLA-16-250) and pellets were stored at −20 °C until further use. The cells were suspended in a lysis buffer (20 mM Tris−HCl, 0.5 mM NaCl, 5 mM imidazole, pH 7.5) and passed five times through an EmulsiFlex-C5 high pressure homogenizer (Avestin). An extra batch of cells were lysed using sonication to exclude the possibility of pressure-induced unfolding of the protein. The cells were thus sonicated at 20% power and a pulse sequence of 5 on, 10 off with a Bandelin Sonoplus sonicator and a UW 2200 tip. The lysate was centrifuged at 35,000*g* for 50 min (Beckman Coulter Avanti, rotor: JA-20). The centrifuged lysate was loaded on the Ni-sepharose affinity chromatography column (HisTrap FF, 5 mL, GE Healthcare). The column was washed with 10 column volumes (CV) of 10% buffer B (20 mM Tris−HCl (pH 7.5), 0.5 M NaCl, 500 mM Imidazole) to wash out nonspecifically bound protein. The His-tagged protein was eluted with a 10−100% linear gradient of buffer B in 20 CV. The eluate was collected and incubated with thrombin (GE Healthcare) overnight at 4 °C.

https://doi.org/10.1021/acsomega.1c06668
ACS Omega 2022, 7, 6184−6194

Table 4. Data Collection and Refinement Statistics Related to Figure 2

	WT *Sc*SLAC	M298L	M298F	M198F/M298F
		Data Collection		
wavelength (Å)	1.5419	0.97917	0.97820	0.97917
space group	$P2_13$	$P2_13$	$P2_13$	$P2_13$
unit cell (*a*,*b*,*c*) (Å)	176.98	177.2	177.62	178.64
resolution range (Å)[a]	29.5−2.7 (2.79−2.70)	72.34−2.19 (2.23−2.19)	30−2.2 (2.26−2.2)	29.77−2.0 (2.03−2.0)
total reflections	376482	543286	808727	2518974
unique reflections	50726	94266	92609	128318
multiplicity	7.4 (7.4)	5.8 (6.0)	8.7 (4.3)	19.6 (20.2)
completeness (%)	99.9 (99.6)	99.2 (99.5)	98.1 (86.3)	100.0 (99.8)
mean I/sigma (I)	10.1 (3.0)	7.1 (2.6)	16.50 (1.69)	24.6 (4.7)
R-merge (%)[b]	15.4 (69.5)	14.8 (65.3)	8.5 (80.5)	8.1 (67.3)
R-meas (%)	18.0 (81.3)	17.8 (79.2)	9.0 (90.7)	8.5 (70.8)
CC1/2	0.995 (0.899)	0.987 (0.750)	99.9 (65.2)	0.999 (0.939)
		Refinement		
resolution (Å)	29.5−2.7	62.65−2.2	29.2−2.2	29.77−2.0
number of reflections	50,613	94,160	92,558	128,253
R-work	20.0	15.2	17.1	14.6
R-free[c]	22.2	16.2	18.5	15.8
number of atoms	4645	4983	4618	5078
protein	4284	4472	4397	4386
Cu	6	8	8	8
water	355	503	213	658
other	0	0	0	26
		Average *B*-Factor		
macromolecules	35.2	31.2	41.6	31.5
Cu	40.2	39.8	64.8	33.9
solvent	39.9	44.2	43.0	43.3
RMS (bond lengths)	0.008	0.007	0.009	0.007
RMS (bond angles)	0.932	0.886	1.190	0.883
favored (%)	96.73	97.68	97.49	97.86
allowed (%)	3.27	2.32	2.33	2.14
outliers (%)	0	0	0.18	0
rotamer outliers (%)	1.58	1.29	0	0.88
clashscore	3.84	4.95	3.86	1.98
PDB code	7BDN	7B4Y	7B2K	7BFM

[a]Highest resolution shell is shown in parenthesis. [b]*R*-merge = $\Sigma|(I_i - \langle I_i\rangle|\Sigma I_i$ where I_i = intensity of the *i*th reflection and $\langle I_i\rangle$ = mean intensity. [c]*R*-factor = $\Sigma(|F_{obs}| - k|F_{calc}|)/\Sigma|F_{obs}|$ and *R*-free is the *R* value for a test set of reflections consisting of a random 5% of the diffraction data not used in refinement.

Five molar equivalents of copper were added to the sample and incubated for 1 h. The sample was then desalted (HiPrep 26/10 Desalting, GE Healthcare) and further purified with anion exchange chromatography (HiTrap DEAE FF, 5 mL, GE Healthcare). The enzyme was subsequently desalted and concentrated (Vivaspin Turbo 15, MWCO 10K, Sartorius). Protein concentration was determined at λ = 280 nm using ε = 43,890 M^{-1} cm^{-1} (UV-2700 UV−Vis Spectrophotometer, Shimadzu).

Kinetics. Oxidation of substrates was monitored with a UV-2700 spectrophotometer (Shimadzu) in a 1 mL plastic cuvette at 42 °C using a temperature-controlled cell holder (TCC-100, Shimadzu). The optimal pH was determined for every substrate and the following parameters were used: (1) 0.1−25 mM ABTS pH 5.0 (λ = 420 nm; ε = 36,000 M^{-1} cm^{-1}), 0.25−15 mM DMP pH 8.0 (λ = 470 nm; ε = 14,800 M^{-1} cm^{-1}), 0.025−1 mM pyrogallol pH 8.5 (λ = 420 nm; ε = 2640 M^{-1} cm^{-1}), and 0.025−2 mM hydrocoerulignone pH 8.5 (λ = 475 nm; ε = 53,200 M^{-1} cm^{-1}). The ABTS stock solution was prepared in double deionized water, DMP and pyrogallol were dissolved in dimethylformamide and hydrocoerulignone in DMSO. Kinetic constants were calculated by fitting data to Michaelis−Menten or substrate inhibition equations (Origin 2018b, Northampton, MA, USA).

Thermostability of ScSLAC and Its Mutants. Enzyme stock solutions (in 20 mM Tris−HCl 0.1 M NaCl pH 7.5) were incubated at 50, 60, 70, 80, and 90 °C. Enzyme solutions were then diluted 500 times into a 1 mL plastic cuvette containing 2 mM ABTS and 50 mM sodium acetate buffer at pH 5.0 (ScSLAC, M298F, and M298L) or pH 4.5 (M198F M298F) at 42 °C. Residual activity of the enzymes were measured at different time points by monitoring the oxidation of 2 mM ABTS at 420 nm.

Protein Crystallization. Both wild-type and mutants of *Sc*SLAC were crystallized using the hanging drop vapor diffusion method at 20 °C. In case of wild type enzymes and single mutants (M298F and M298L), the mother liquor was composed of 40% MPD, 200 mM NH_4−OAc and 100 mM HEPES (pH 7.5) and was mixed with protein (20 mg/mL in 20 mM Tris−HCl buffer) in a 1:2 ratio. Crystals with approximate dimensions of 300 × 300 × 300 μm were formed in 48 h after incubation in a vibration free crystallization

https://doi.org/10.1021/acsomega.1c06668
ACS Omega 2022, 7, 6184−6194

incubator (Molecular Dimensions, Sheffield, UK). The double mutant of ScSLAC (M198F-M298F) was crystallized similarly, where the mother liquor was composed of 40% PEG400, 200 mM Li_2SO_4, and 100 mM Tris−HCl (pH 8.5). Prior to data collection, crystals were vitrified in liquid nitrogen without any additional cryoprotectants.

Data Collection and Structure Determination. The diffraction data for the wild type enzyme was recorded on a Rigaku Compact HomeLab diffractometer with a MicroMax-003 sealed-tube Cu-anode source (1.54 Å radiation), a 4-circle partial-chi goniometer, and a Saturn 944 + CCD detector. The crystals diffracted to 2.7 Å resolution and conformed to the $P2_13$ space group. Similarly, crystals of the mutant versions of the enzyme also conformed to the $P2_13$ space group. The diffraction data for M298L and M198F-M298F double mutant were collected on a BL13-XALOC beamline at the ALBA Synchrotron light source (Barcelona, Spain) to a resolution of 2.2 and 2.0 Å resolution, respectively, on a Dectris Pilatus 6M detector. For M298F, the data set diffracting to 2.2 Å resolution was collected on the F1 beamline at the Cornell High Energy Synchrotron Source (Ithaca, NY, USA) using an ADSC Quantum 270 detector. Diffraction intensities were integrated with XDS[42] and scaled with Aimless.[43] For structure determination of all respective structures, the molecular replacement with PHASER[44] was carried out, using input diffraction data, sequence information, and the atomic coordinates of the previously deposited structure of *Sc*SLAC (PDB ID 3CG8). To minimize phase bias in the generated electron density maps, sites containing mutations in the search model were truncated to β-carbon. Iterative cycles of manual and automatic refinement with COOT[45] and PHENIX[46] were carried out. Crystallographic statistics are summarized in Table 4.

Small-Angle X-ray Scattering. SAXS data were collected on CHESS beamline id7a at 8.667 keV (1.431 Å) at 1 × 1012 photons/s. The 250 × 250 μm diameter X-ray beam is centered on a 1.5 mm diameter capillary sample cell having 10 μm thick quartz glass walls (Charles Supper Company, Natik, MA). Sample cell and X-ray flight path, including beamstop, were kept in vacuo ($<1 \times 10^{-3}$ torr) to eliminate air scatter. The temperature of the cell was maintained at 4 °C. Images were collected on a Pilatus 100K-S detector (Dectris, Baden, Switzerland). The sample-to-detector distance was calibrated using silver behenate powder (The Gem Dugout, State College, PA). The q-space range ($4\pi \sin \theta/\lambda$ with 2θ being the scattering angle) reached from q_{min} = 0.009 $Å^{-1}$ to q_{max} = 0.24 Å-1. Image integration, normalization, and subtraction were carried out using the BioXTAS RAW program.[47] The radiation damage assessment was based on the CORMAP criterion as implemented in RAW.[48] Sample and buffer solutions were normalized to equivalent exposure before subtraction using transmitted intensity recorded from a beamstop diode.

Chromatographic separation of samples was conducted at 4 °C using a Superdex Increase 200 10/300 column on an AKTA Pure system (GE Healthcare Life Sciences, Marlborough, MA). The flow rate into the sample cell was 0.6 mL/min with 1 s exposures taken continuously.

■ ASSOCIATED CONTENT

Supporting Information

The Supporting Information is available free of charge at https://pubs.acs.org/doi/10.1021/acsomega.1c06668.

Experimental setup of size-exclusion chromatography coupled SAXS and the heat inactivation profiles of wild-type and mutant laccases; SAXS chromatogram showing integrated SAXS intensity as a function of elution for 5 ScSLAC samples; Guinier analysis of the ScSLAC samples; heat inactivation profiles for wild-type and mutant ScSLAC variants; and SAXS data collection parameters (PDF)

■ AUTHOR INFORMATION

Corresponding Author

Tiit Lukk − *Department of Chemistry and Biotechnology, Tallinn University of Technology, Tallinn 12618, Estonia;* orcid.org/0000-0001-7765-1707; Email: tiit.lukk@taltech.ee

Authors

Kairit Zovo − *Department of Chemistry and Biotechnology, Tallinn University of Technology, Tallinn 12618, Estonia*

Hegne Pupart − *Department of Chemistry and Biotechnology, Tallinn University of Technology, Tallinn 12618, Estonia*

Arie Van Wieren − *Department of Chemistry, Biochemistry, Physics and Engineering, Indiana University of Pennsylvania, Indiana, Pennsylvania 15705, United States*

Richard E. Gillilan − *MacCHESS (Macromolecular Diffraction Facility at CHESS), Cornell University, Ithaca, New York 14850, United States*

Qingqiu Huang − *MacCHESS (Macromolecular Diffraction Facility at CHESS), Cornell University, Ithaca, New York 14850, United States*

Sudipta Majumdar − *Department of Chemistry, Biochemistry, Physics and Engineering, Indiana University of Pennsylvania, Indiana, Pennsylvania 15705, United States*

Complete contact information is available at: https://pubs.acs.org/10.1021/acsomega.1c06668

Author Contributions

The manuscript was written through contributions of all authors. All authors have given approval to the final version of the manuscript. T.L., R.E.G. and S.M. designed research; K.Z., H.P., A.v.W., R.E.G., Q.H., S.M., and T.L. performed research; K.Z., H.P., R.E.G., and T.L. analyzed data; K.Z., R.E.G, S.M., and T.L. wrote the manuscript.

Funding

This work was supported by the European Regional Development Fund and the programme Mobilitas Pluss (MOBTT60).

Notes

The authors declare no competing financial interest.

■ ACKNOWLEDGMENTS

The authors would like to thank Dr. Maria Kulp for helpful discussions during the preparation of this manuscript. X-ray diffraction experiments were performed at BL13-XALOC beamline at ALBA Synchrotron Light Facility with the collaboration of ALBA staff and at the Center for High Energy X-ray Sciences (CHEXS), which was supported by the National Science Foundation under award DMR-1829070, and the Macromolecular Diffraction at CHESS (MacCHESS) facility, which was supported by award 1-P30-GM124166-01A1 from the National Institute of General Medical Sciences, National Institutes of Health, and by New York State's Empire State Development Corporation (NYSTAR).

ABBREVIATION

*Sc*SLAC, *Streptomyces coelicolor* small laccase; ABTS, 2,2′-azino-bis-(3-ethylbenzothiazoline-6-sulphonic acid); DMP, 2,6-dimethoxyphenol; HCL, hydrocoerulignone; IPTG, isopropyl-β-D-thiogalactopyranoside; DMSO, dimethyl sulfoxide

REFERENCES

(1) Giardina, P.; Faraco, V.; Pezzella, C.; Piscitelli, A.; Vanhulle, S.; Sannia, G. Laccases: a never-ending story. *Cell. Mol. Life Sci.* **2010**, *67*, 369−385.

(2) Jones, S. M.; Solomon, E. I. Electron transfer and reaction mechanism of laccases. *Cell. Mol. Life Sci.* **2015**, *72*, 869−883.

(3) Rodgers, C. J.; Blanford, C. F.; Giddens, S. R.; Skamnioti, P.; Armstrong, F. A.; Gurr, S. J. Designer laccases: a vogue for high-potential fungal enzymes? *Trends Biotechnol.* **2010**, *28*, 63−72.

(4) Dwivedi, U. N.; Singh, P.; Pandey, V. P.; Kumar, A. Structure-function relationship among bacterial, fungal and plant laccases. *J. Mol. Catal. B Enzym.* **2011**, *68*, 117−128.

(5) Sharma, A.; Jain, K. K.; Jain, A.; Kidwai, M.; Kuhad, R. C. Bifunctional in vivo role of laccase exploited in multiple biotechnological applications. *Appl. Microbiol. Biotechnol.* **2018**, *102*, 10327−10343.

(6) Sakurai, T.; Kataoka, K. Structure and function of type I copper in multicopper oxidases. *Cell. Mol. Life Sci.* **2007**, *64*, 2642−2656.

(7) Warren, J. J.; Lancaster, K. M.; Richards, J. H.; Gray, H. B. Inner- and outer-sphere metal coordination in blue copper proteins. *J. Inorg. Biochem.* **2012**, *115*, 119−126.

(8) Sitarz, A. K.; Mikkelsen, J. D.; Meyer, A. S. Structure, functionality and tuning up of laccases for lignocellulose and other industrial applications. *Crit. Rev. Biotechnol.* **2016**, *36*, 70−86.

(9) Machczynski, M. C.; Vijgenboom, E.; Samyn, B.; Canters, G. W. Characterization of SLAC: A small laccase fromStreptomyces coelicolorwith unprecedented activity. *Protein Sci.* **2004**, *13*, 2388−2397.

(10) Skálová, T.; Dohnálek, J.; Østergaard, L. H.; Østergaard, P. R.; Kolenko, P.; Dušková, J.; Štěpánková, A.; Hašek, J. The Structure of the Small Laccase from Streptomyces coelicolor Reveals a Link between Laccases and Nitrite Reductases. *J. Mol. Biol.* **2009**, *385*, 1165−1178.

(11) Guan, Z.-B.; Luo, Q.; Wang, H.-R.; Chen, Y.; Liao, X.-R. Bacterial laccases: promising biological green tools for industrial applications. *Cell. Mol. Life Sci.* **2018**, *75*, 3569−3592.

(12) Mate, D. M.; Alcalde, M. Laccase: a multi-purpose biocatalyst at the forefront of biotechnology. *Microb. Biotechnol.* **2017**, *10*, 1457−1467.

(13) Chandra, R.; Chowdhary, P. Properties of bacterial laccases and their application in bioremediation of industrial wastes. *Environ. Sci.: Processes Impacts* **2015**, *17*, 326−342.

(14) Fillat, Ú.; Ibarra, D.; Eugenio, M.; Moreno, A.; Tomás-Pejó, E.; Martín-Sampedro, R. Laccases as a Potential Tool for the Efficient Conversion of Lignocellulosic Biomass: A Review. *Fermentation* **2017**, *3*, 17.

(15) Mate, D. M.; Alcalde, M. Laccase engineering: From rational design to directed evolution. *Biotechnol. Adv.* **2015**, *33*, 25−40.

(16) Munk, L.; Sitarz, A. K.; Kalyani, D. C.; Mikkelsen, J. D.; Meyer, A. S. Can laccases catalyze bond cleavage in lignin? *Biotechnol. Adv.* **2015**, *33*, 13−24.

(17) Prins, A.; Kleinsmidt, L.; Khan, N.; Kirby, B.; Kudanga, T.; Vollmer, J.; Pleiss, J.; Burton, S.; Le Roes-Hill, M. The effect of mutations near the T1 copper site on the biochemical characteristics of the small laccase from Streptomyces coelicolor A3(2). *Enzyme Microb. Technol.* **2015**, *68*, 23−32.

(18) Sherif, M.; Waung, D.; Korbeci, B.; Mavisakalyan, V.; Flick, R.; Brown, G.; Abou-Zaid, M.; Yakunin, A. F.; Master, E. R. Biochemical studies of the multicopper oxidase (small laccase) from S treptomyces coelicolor using bioactive phytochemicals and site-directed mutagenesis. *Microb. Biotechnol.* **2013**, *6*, 588−597.

(19) Xu, R.; Zhang, K.; Liu, P.; Han, H.; Zhao, S.; Kakade, A.; Khan, A.; Du, D.; Li, X. Lignin depolymerization and utilization by bacteria. *Bioresour. Technol.* **2018**, *269*, 557−566.

(20) Hämäläinen, V.; Grönroos, T.; Suonpää, A.; Heikkilä, M. W.; Romein, B.; Ihalainen, P.; Malandra, S.; Birikh, K. R. Enzymatic Processes to Unlock the Lignin Value. *Front. Bioeng. Biotechnol.* **2018**, *6*, 20.

(21) Majumdar, S.; Lukk, T.; Solbiati, J. O.; Bauer, S.; Nair, S. K.; Cronan, J. E.; Gerlt, J. A. Roles of Small Laccases from Streptomyces in Lignin Degradation. *Biochemistry* **2014**, *53*, 4047−4058.

(22) Singh, R.; Hu, J. G.; Regner, M. R.; Round, J. W.; Ralph, J.; Saddler, J. N.; Eltis, L. D. Enhanced delignification of steam-pretreated poplar by a bacterial laccase. *Sci. Rep.* **2017**, *7*, 42121.

(23) Lee, S.; Kang, M.; Bae, J. N.; Sohn, J. N.; Sung, B. H. Bacterial Valorization of Lignin: Strains, Enzymes, Conversion Pathways, Biosensors, and Perspectives. *Front. Bioeng. Biotechnol.* **2019**, *7*, 209.

(24) Durão, P.; Bento, I.; Fernandes, A. T.; Melo, E. P.; Lindley, P. F.; Martins, L. O. Perturbations of the T1 copper site in the CotA laccase from Bacillus subtilis: structural, biochemical, enzymatic and stability studies. *J. Biol. Inorg Chem.* **2006**, *11*, 514−526.

(25) Hong, G.; Ivnitski, D. M.; Johnson, G. R.; Atanassov, P.; Pachter, R. Design Parameters for Tuning the Type 1 Cu Multicopper Oxidase Redox Potential: Insight from a Combination of First Principles and Empirical Molecular Dynamics Simulations. *J. Am. Chem. Soc.* **2011**, *133*, 4802−4809.

(26) Maté, D.; García-Burgos, C.; García-Ruiz, E.; Ballesteros, A. O.; Camarero, S.; Alcalde, M. Laboratory Evolution of High-Redox Potential Laccases. *Chem. Biol.* **2010**, *17*, 1030−1041.

(27) Toscano, M. D.; De Maria, L.; Lobedanz, S.; Østergaard, L. H. Optimization of a Small Laccase by Active-Site Redesign. *Chembiochem* **2013**, *14*, 1209−1211.

(28) Zhu, Y.; Zhang, Y.; Zhan, J.; Lin, Y.; Yang, X. Axial bonds at the T1 Cu site of Thermus thermophilus SG 0.5 JP 17-16 laccase influence enzymatic properties. *FEBS Open Bio* **2019**, *9*, 986−995.

(29) Galli, C.; Gentili, P.; Jolivalt, C.; Madzak, C.; Vadalà, R. How is the reactivity of laccase affected by single-point mutations? Engineering laccase for improved activity towards sterically demanding substrates. *Appl. Microbiol. Biotechnol.* **2011**, *91*, 123−131.

(30) Olbrich, A. C.; Schild, J. N.; Urlacher, V. B. Correlation between the T1 copper reduction potential and catalytic activity of a small laccase. *J Inorg Biochem* **2019**, *201*, 110843.

(31) Hall, J. F.; Kanbi, L. D.; Strange, R. W.; Hasnain, S. S. Role of the Axial Ligand in Type 1 Cu Centers Studied by Point Mutations of Met148 in Rusticyanin. *Biochemistry* **1999**, *38*, 12675−12680.

(32) Berry, S. M.; Ralle, M.; Low, D. W.; Blackburn, N. J.; Lu, Y. Probing the Role of Axial Methionine in the Blue Copper Center of Azurin with Unnatural Amino Acids. *J. Am. Chem. Soc.* **2003**, *125*, 8760−8768.

(33) Gupta, A.; Nederlof, I.; Sottini, S.; Tepper, A. W. J. W.; Groenen, E. J. J.; Thomassen, E. A. J.; Canters, G. W. Involvement of Tyr108 in the Enzyme Mechanism of the Small Laccase from Streptomyces coelicolor. *J. Am. Chem. Soc.* **2012**, *134*, 18213−18216.

(34) Li, H.; Webb, S. P.; Ivanic, J.; Jensen, J. H. Determinants of the relative reduction potentials of type-1 copper sites in proteins. *J. Am. Chem. Soc.* **2004**, *126*, 8010−8019.

(35) Gunne, M.; Höppner, A.; Hagedoorn, P.-L.; Urlacher, V. B. Structural and redox properties of the small laccase Ssl1 fromStreptomyces sviceus. *FEBS J.* **2014**, *281*, 4307−4318.

(36) Ducros, V.; Brzozowski, A. M.; Wilson, K. S.; Brown, S. H.; Østergaard, P.; Schneider, P.; Yaver, D. S.; Pedersen, A. H.; Davies, G. J. Crystal structure of the type-2 Cu depleted laccase from Coprinus dnereus at 2.2 Å resolution. *Nat. Struct. Biol.* **1998**, *5*, 310−316.

(37) Piontek, K.; Antorini, M.; Choinowski, T. Crystal Structure of a Laccase from the FungusTrametes versicolor at 1.90-Å Resolution Containing a Full Complement of Coppers. *J. Biol. Chem.* **2002**, *277*, 37663−37669.

(38) Skálová, T.; Dušková, J.; Hašek, J.; Štěpánková, A.; Koval, T.; Østergaard, L. H.; Dohnálek, J. Structure of laccase fromStreptomyces coelicolorafter soaking with potassium hexacyanoferrate and at an

https://doi.org/10.1021/acsomega.1c06668
ACS Omega 2022, 7, 6184−6194

improved resolution of 2.3 Å. *Acta Crystallogr., Sect. F: Struct. Biol. Cryst. Commun.* **2011**, *67*, 27−32.
(39) Marshall, N. M.; Garner, D. K.; Wilson, T. D.; Gao, Y.-G.; Robinson, H.; Nilges, M. J.; Lu, Y. Rationally tuning the reduction potential of a single cupredoxin beyond the natural range. *Nature* **2009**, *462*, 113−116.
(40) Keedy, D. A.; Kenner, L. R.; Warkentin, M.; Woldeyes, R. A.; Hopkins, J. B.; Thompson, M. C.; Brewster, A. S.; Van Benschoten, A. H.; Baxter, E. L.; Uervirojnangkoorn, M.; McPhillips, S. E.; Song, J.; Alonso-Mori, R.; Holton, J. M.; Weis, W. I.; Brunger, A. T.; Soltis, S. M.; Lemke, H.; Gonzalez, A.; Sauter, N. K.; Cohen, A. E.; van den Bedem, H.; Thorne, R. E.; Fraser, J. S. Mapping the conformational landscape of a dynamic enzyme by multitemperature and XFEL crystallography. *Elife* **2015**, *4*, No. e07574.
(41) Schroer, M. A.; Paulus, M.; Jeworrek, C.; Krywka, C.; Schmacke, S.; Zhai, Y.; Wieland, D. C. F.; Sahle, C. J.; Chimenti, M.; Royer, C. A.; Garcia-Moreno, B.; Tolan, M.; Winter, R. High-pressure SAXS study of folded and unfolded ensembles of proteins. *Biophys. J.* **2010**, *99*, 3430−3437.
(42) Kabsch, W. Automatic Processing of Rotation Diffraction Data from Crystals of Initially Unknown Symmetry and Cell Constants. *J. Appl. Crystallogr.* **1993**, *26*, 795−800.
(43) Winn, M. D.; Ballard, C. C.; Cowtan, K. D.; Dodson, E. J.; Emsley, P.; Evans, P. R.; Keegan, R. M.; Krissinel, E. B.; Leslie, A. G. W.; McCoy, A.; McNicholas, S. J.; Murshudov, G. N.; Pannu, N. S.; Potterton, E. A.; Powell, H. R.; Read, R. J.; Vagin, A.; Wilson, K. S. Overview of theCCP4 suite and current developments. *Acta Crystallogr., Sect. D: Struct. Biol.* **2011**, *67*, 235−242.
(44) Mccoy, A. J.; Grosse-Kunstleve, R. W.; Adams, P. D.; Winn, M. D.; Storoni, L. C.; Read, R. J. Phasercrystallographic software. *J. Appl. Crystallogr.* **2007**, *40*, 658−674.
(45) Emsley, P.; Lohkamp, B.; Scott, W. G.; Cowtan, K. Features and development ofCoot. *Acta Crystallogr., Sect. D: Biol. Crystallogr.* **2010**, *66*, 486−501.
(46) Adams, P. D.; Grosse-Kunstleve, R. W.; Hung, L.-W.; Ioerger, T. R.; McCoy, A. J.; Moriarty, N. W.; Read, R. J.; Sacchettini, J. C.; Sauter, N. K.; Terwilliger, T. C. PHENIX: building new software for automated crystallographic structure determination. *Acta Crystallogr., Sect. D: Struct. Biol.* **2002**, *58*, 1948−1954.
(47) Hopkins, J. B.; Gillilan, R. E.; Skou, S. BioXTAS RAW: improvements to a free open-source program for small-angle X-ray scattering data reduction and analysis. *J. Appl. Crystallogr.* **2017**, *50*, 1545−1553.
(48) Franke, D.; Jeffries, C. M.; Svergun, D. I. Correlation Map, a goodness-of-fit test for one-dimensional X-ray scattering spectra. *Nat. Methods* **2015**, *12*, 419−422.

https://doi.org/10.1021/acsomega.1c06668
ACS Omega 2022, 7, 6184−6194